EFFECT OF NANOSIZING OF MATERIALS ON LIVING ORGANISM

F.Watari*, S.Abe, C.Koyama, S.Inoue, T.Akasaka, M.Uo, M.Matsuoka, N.Takashi, Y.Totsuka, E.Hirata, A.Yokoyama, M.Esaki, M.Morita and T.Yonezawa[1]

Graduate School of Dental Medicine, Hokkaido University, Sapporo 060-8586, JAPAN
[1]Department of Chemistry, School of Science, The University of Tokyo, Tokyo, 113-0033, JAPAN
E-mail: watari@den.hokudai.ac.jp

Abstract

Biological effect of nanosizing of materials was investigated by both in vitro biochemical cell functional test and in vivo animal implantation test. Dependence of reaction of cells and tissue, and that of bone formation of apatite on particle size were studied. The increase of specific surface area causes the enhancement of chemical reactivity and toxicity for stimulative materials, which is most usually and easily recognized. However even for biocompatible materials, stimulus was increased with the decrease of particle size and pronounced below 10 μm where phagocytosis was induced to cells and inflammation to tissue. For the size below 50nm, particles invade into the internal body through the respiratory or digestive system and diffuse inside body.

Although the particle size of carbon nanotube (CNT) allows the possibility to attain pulmonary alveolus through the respiratory system similarly to asbestos, the chemical properties and bio-environmental behavior seem different. We have rather found the favorite properties as biomaterials such as affinity for saccharides and proteins, cell adhesion, and apatite precipitation.

Macroscopic hydroxyapatite, which exhibits excellent osteoconductivity, cannot be substituted with natural bone, while nanoapatite composite with collagen showed resorption due to phagocytosis by osteoclasts and new bone formation by osteoblasts when implanted and leads to the bone substitutional properties. Thus nanosizing induces the intrinsic functions of biological organism and results in the conversion of functions such as from biocompatibility to stimulus and from non-bone substitutional to bone substitutional through biological process.

Introduction

The development of nanotechnology has been affecting a large influence on human life. Completion of genome analysis has brought the post-genome era to enable application for the biological and medical purpose. The reaction of biological organism to proteins and saccharides including virus, bacteria, enzyme, and phamacological agents has been investigated in biology and medicine. For materials the reaction to the usual cases, that is, the macroscopic size is well investigated. However the effect of micro/nanosizing of materials onto biological organism has been little understood. Nanosizing of materials brings in quantum effect for less than about 1.5 nm and the formation of activity sites such as seen in some catalysts. However the most unambiguous and influential effect is the surface area effect. It is well-known that the specific surface area which is defined as surface area for unit volume is increased with the decrease of particle size and chemical reactivity is pronounced. Therefore high throughput is expected in the functions and performances of material properties and devices.

One of the most important factors to affect on the biocompatibility of materials is ionic dissolution, which is closely related to the specific surface area. This is also true for micro and nano size, and becomes apparent very often as stimulus and toxicity for nanosizing effect. Nanosizing effect which affects on biocompatibility is usually interpreted from this aspect.

On the other hand, corrosion-resistent and biocompatible Ti causes inflammation in abraded fine particles [1, 2] which are produced from artificial joint, and asbestos [3], a kind of clay minerals, induces mesothelioma after a long-term, large quantity of exposure. These phenomena cannot be explained by the specific surface area effect and understood as the different effect, that is, physical size and shape effect, apart from the material properties of either toxicity or biocompatibility. The abraded fine particles may diffuse inside the body through the cardiovascular system. There is also the possibility that the uptake of nanoparticles occurs through the respiratory and digestive systems.

Meanwhile Drug Delivery System (DDS) is one of the most typical biomedical applications of nanoparticles. The development of DDS is expected for the administration of anticancer agent and gene transfection. The behavior of nanoparticles in the internal body is necessary to investigate for the assessment of nanotoxicology which may be regarded as the demerit side of nanoparticles but this is, in turn, essential to comprehend the behavior of DDS and confirm the path to reach the diseased target which may be regarded as merit side.

As another typical subject of nanomaterials, much attention has been paid to carbon nanotubes (CNT) up to now due to their unique structure and properties. The development for the application in the electronic and

chemical fields such as field emission electron gun and hydrogen storage materials has been intensively done. However the application for the biomedical field has been very rare. There are arguments that CNT may have the serious toxicity due to its acicular or fibrous particle shape, associated with lung carcinogenicity of asbestos. Asbestos induces mesothelioma after a long-term, large quantity of exposure, although it is a silicate in composition, a kind of clay minerals. There is a possibility to pass through bronchial in the respiratory system for the particles with the size below 10μm. Both CNT and asbestos have the fibrous to acicular particle form, and the particle size is less than 1μm in diameter and ranged in nm to tens of μm in length. From this point of view there is a possibility to reach pulmonary alveolus through the respiratory system for some of both CNT and asbestos particles.

Hydroxyapatite (HAP), the main component of bone, has the difference in behavior between synthetic apatite and bone. Synthetic hydroxyapatite, in the usual case, of a macroscopic size, exhibits excellent osteoconductivity. However it is not substituted to natural bone and remains permanently in the body. Natural bone is composed of collagen and nanocrystallites of apatite with the size of approximately 50nm. Bone is continuously remodeled by resorption and new bone formation. Then there exist apatites with the different behavior, non-resorbable and resorbable apatite.

Thus nanosizing causes different behavior from macroscopic size for biocompatible materials [4]. These strongly suggest the necessity to reveal the micro/nanosizing effect of materials onto living organism. In the present study both biochemical cell functional test and animal implantation test were done to clarify the micro/nanosizing effect and particle size dependence of reaction of cells and tissue [5, 6]. The behavior of invasion of nanoparticles and internal diffusion inside body was visualized using XSAM (X-ray Scanning Analytical Microscope) [7, 8] for the level of the whole body and organs. The assessment of CNTs in comparison with asbestos and development for biomedical applications were also done. Then the nanosizing effect in apatite was investigated using biomimetic bone-resembling nanoapatite/collagen composite and the mechanism of the different behavior from macroscopic apatite was discussed.

Experimental

1. Specimens

99.9% pure Ti, and TiO_2 particles of the various size were principally used throughout. For in vitro and in vivo implantation tests Fe, Ni, TiO_2 and carbon nanotubes were also used. The particles of nominal size from 500 nm to 150 μm were used for Ti. To reduce the size distribution as small as possible and equalize the experimental conditions between materials such as metallic Ti, Fe and Ni, the particles of 0.5, 3, 10 μm were extracted by sedimentation method and those less than 300 nm were extracted by ultrafiltration.

2. Dissolution test of Ti particles

After Ti particles were immersed in HBSS (Hanks balanced salt solution) at 37°C for 1 month, the supernatant was filtered through a 0.45 μm membrane to remove Ti particles and then elemental analysis was done by Inductively Coupled Plasma - Atomic Emission Spectrometry (ICP-AES) using ICPS-8100, Shimazu, Tokyo, Japan.

3. Biochemical analyses of cellular reaction to materials

Human neutrophils, which play a central role in the initial stage of inflammation in a non-specific manner against foreign bodies, were used as probes. Particles smaller (0.5, 3 μm) and larger (10, 50, 150 μm) than the neutrophils were used to determine the relationship between cell and particle size with respect to cytotoxicity.

Cell survival rate and lactate dehydrogenase (LDH) values, superoxide anion (O^{2-}) production per 106 neutrophils were measured. Cytokines of TNF-α and Il-1ß were measured using ELISA kits (Endogen, Inc. USA). Morphological change of neutrophils mixed with HBSS containing various particles was observed by optical microscopy (OM: Zeiss, Axioskop, Germany) and scanning electron microscopy (SEM: Hitachi S-4300, Tokyo, Japan).

4. Animal experiments

Particles were inserted in the subcutaneous connective tissue in the abdominal region of Wistar rats aged between 11 and 12 weeks (weight 350-380 g). Specimens were prepared through the usual process of fixation, embedding, sectioning, staining with hematoxylin-eosin, and histopathologically observed.

5. Visualization of internal distribution of nanoparticles

The compulsory exposure test to the respiratory system was performed to rats using 30 nm TiO_2 particles. The uptake of nanoparticles through the digestive system was also tested for mice by mixing agar gelatin containing 30 nm TiO_2 particles to their foods. To inspect internal diffusion more simply, the experiments were done for mice by injecting nanoparticles directly to the cardiovascular system to caudal vein. The observation of internal distribution of nanoparticles was conducted for the whole body and each organ by elemental mapping in air using X-ray Scanning Analytical Microscope (XSAM: Horiba XGT-2000V, Tokyo,

Japan) without the pretreatments of fixation, dehydration and staining after sectioning. The distribution inside the organ was inspected by elemental mapping using energy dispersive X-ray spectroscopy (EDS) installed to SEM. The experiments were also done for the particles Ti, Fe, Ni, Pt, TiC, Fe_2O_3.

6. CNT and Asbestos

MWCNTs (multi-wall CNT) of about 5nm in diameter and 20μm in length, synthesized by chemical vapor deposition (NanoLab, Inc. MA, U.S.A.), were used throughout the experiments as well as SWCNTs (single wall CNT) and CNFs (carbon nanofiber) for part of experiments for comparison. They were treated with hydrochloric acid to remove metal catalysts. The purity was about 98 wt %. CNTs were dispersed in the deionized water by sonication for 3 min.

UICC standard specimens of three kinds of the most representative minerals in asbestos were used throughout. They are chrysotile, crocidolite and amosite. For comparison non-asbestos alternative (alumina) was also used.

7. Cell culture

Human osteoblast-like cells (SaOS2) were used for cell culture experiments on CNT. CNT scaffolds were made by vacuum filtration of the dispersed CNT slurry onto porous polycarbonate membranes (PC). Cell culture was done in a usual process.

8. Observation and characterization

Morphology of particles and cells was observed by scanning electron microscopy (SEM:S-4300, HITACHI, Japan) and elemental analysis by energy dispersive X-ray spectroscopy (EDS) was also done. The high resolution observation of CNT was done with Multi-Beam High Voltage Electron Microscope (JEM-ARM-1300, JEOL, Japan) of Center for Advanced Research of Energy Conversion Materials, Hokkaido University at accelerating voltage 1250 kV.

9. Biomimetic nanoapatite/collagen composite

Hydroxyapatite-collagen composites synthesized biomimetically on collagen type I were implanted into the subcutaneous tissue and bone defects in the femur of rats for 1-12 weeks and observed histopathologically [9].

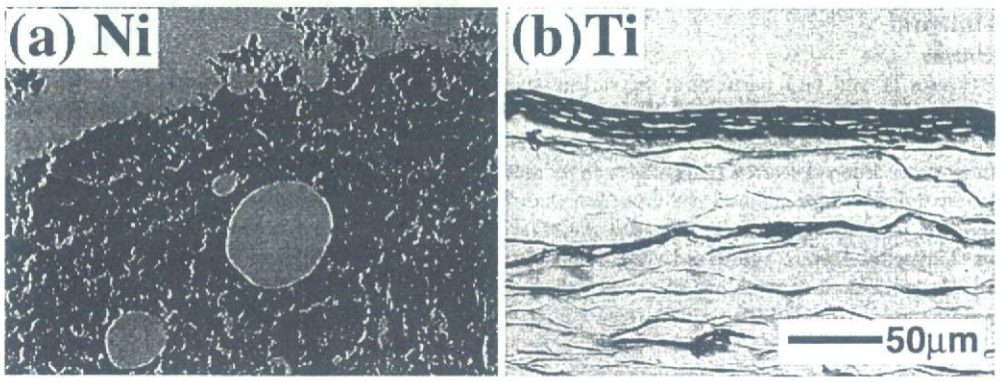

Fig.1 Histological image of rat soft tissue inserted with Ni (a) and Ti (b) of macroscopic size for 1 week.

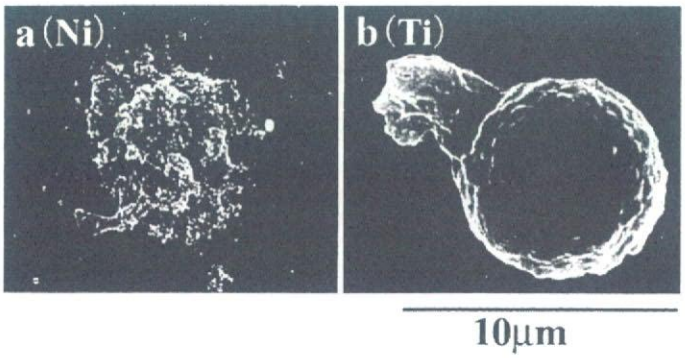

Fig.2 SEM images of human neutrophils exposed to the 500 nm particles of Ni (a) and Ti (b).

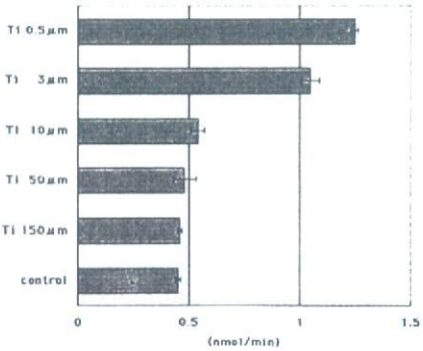

Fig.3 Dependence of superoxide production from neutrophils on Ti particle size [6].

Results

Fig.1 shows the comparison of tissue reaction to the macroscopic size (1 mmφx 10 mm) of Ni (a) and Ti (b) after 1 week implantation in the dorsal thoracic region of rat. Implant had been situated in the upper space of each photograph. In Ni the expansion of capillary vessels was observed. Tissue in the photograph was in necrosis and in degeneration in the distant region. For Ti fibrous connective tissue was already formed surrounding implant from the earlier stage, which is the feature of biocompatible materials [10].

Fig.2 shows the SEM image of human neutrophils exposed to 500nm particles of Ni (a) and Ti (b) in HBSS. The morphology of neutrophils exposed to Ni particles was often transformed or destroyed (a) due to its toxicity. For Ti (b) a neutrophil is extending its pseudopod and going to phagocytize a 500nm Ti particle. For the particles larger than about 10μm, phagocytosis was not observed.

Fig.3 shows the dependence of superoxide production from human neutrophils on Ti particle size , Superoxide was increased with the decrease of particle size. The increase was pronounced for 3μm and 500nm. The release of LDH and cytokines TNF-α and Il-1ß showed the similar behavior as superoxide, while cell survival rate showed the inverse decreasing tendency. Under these conditions ICP elemental analysis indicated that the dissolution from Ti particles was negligible below detection limit [5]. The pronounced phenomena of biochemical cell reaction for below 10μm in Fig.3 are closely related to the phagocytosis shown in Fig.2.

The histological image of in vivo tissue reaction of rat to the different size of Ti particles showed the similar size dependence to those in vitro shown in Figs.2 and 3.

Fig.4 showed the histopathological image of tissue reaction for short-term (1 week) implantation in the subcutaneous tissue of rat for 2 μm Ni and Ti particles. For Ni particles necrosis occurred (Fig.4a) while Ti particles were phagocytized in the cells.

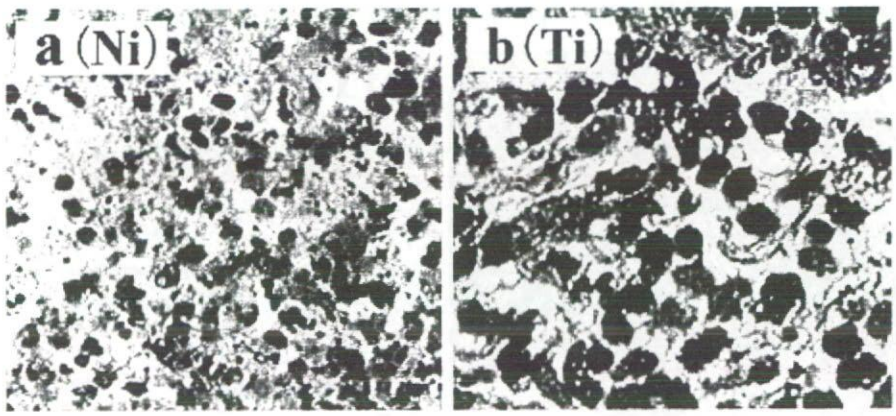

Fig.4 Tissue reaction for short-term implantation to 0.5 μm Ni and 3 μm Ti particles. Necrosis and inflammation occurred respectively.

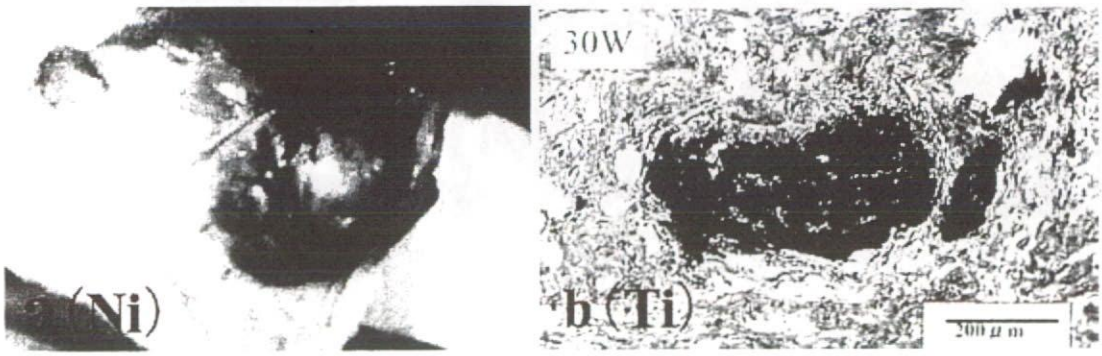

Fig.5 Tissue reaction for long -term implantation to 0.5 μm Ni and 3 μm Ti particles. Tumor induced after 1 year implantation of 0.5 μm Ni particles.

Fig.5 showed the tissue reaction for long-term implantation for 0.5 μm Ni and 3 μm Ti particles. Fig.5a is tumor induced after 1 year implantation of Ni particles in the subcutaneous tissue of rat. Ni is already toxic in a macroscopic size as seen in Fig.1. When it becomes fine particles, toxicity is enhanced remarkably. This is the typical example of specific surface effect which increases reciprocally to particle size and leads to the enhancement of chemical dissolution and therefore toxicity. Fig.5b is the case for 3μm Ti particles after 30 weeks. For this range of particle size the particles originally scattered in tissue in a short term of implantation became gradually agglomerated with the time for the long term by biological process of repeated cycle of phagocytosis and cell death.

Fig.6 shows the dependence of TNF-α release from neutrophils on particle size down to nm size. TNF-α is one of the most representative cytokines related to inflammation. Stimulus, represented as amount of TNF-α release, which is pronounced below 3μm, exhibited the maximum from around μm down to 500nm and then for further smaller size decreased below 200nm. This means that the biophylactic system does not work well any more against the invasion of nanoparticles into the inside of body.

Fig.7 is the Ti mapping of the internal whole body of rats by XSAM after compulsory exposure test to respiratory system, and shows the distribution of 30nm TiO_2 particles. The condensation occurred from the respiratory system to urinary bladder by diffusion in the body through the cardiovascular system after the direct uptake into blood vessels from lung cells.

Fig.8 is the XSAM elemental analysis from spleen for the case after 10 days of oral administration of 30 nm TiO_2 particles. Although peak height is small in this case, Ti-Kα peak undoubtedly exists other than Fe-

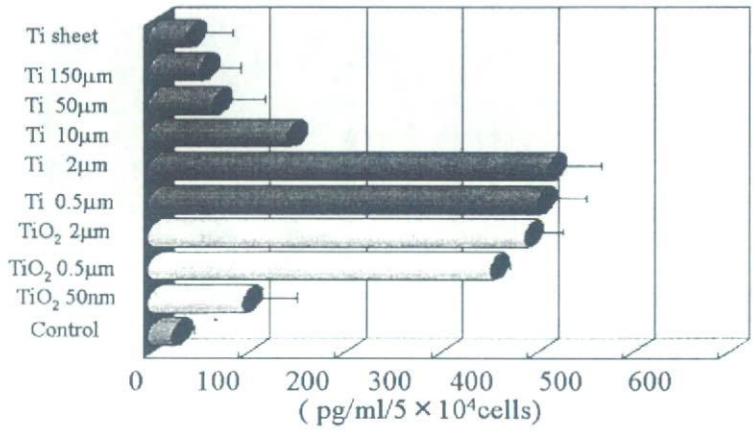

Fig.6 Dependence of TNF-α release from neutrophils on particle size down to nm size [4]

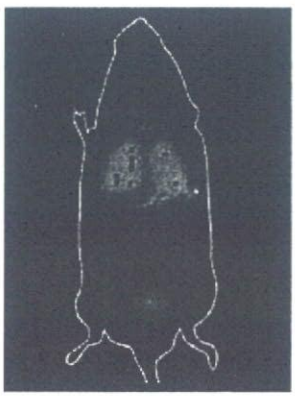

Fig.7 XSAM Ti mapping of internal distribution of 30 nm TiO_2 particles after compulsory exposure test [4].

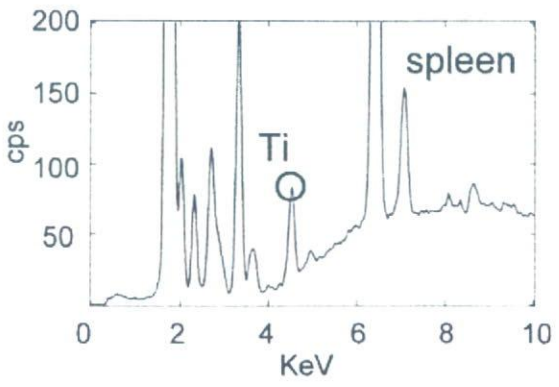

Fig.8 Elemental analysis of spleen after 10 days of oral administration of 30nm TiO_2.

Kα peaks around 6.5 keV and peaks of incident X-ray from Rh target below 4 keV. This confirms the phenomenon that nanoparticles were taken into the internal body through digestion system.

Fig.9 shows the X-ray transmission image and the corresponding Ti elemental mapping by XSAM for 5min and 3hr after injection of 30nm TiO_2 particles to caudal vein. TiO_2 nanoparticles diffused to lung just after injected, then liver and spleen with time course.

Fig.10 shows the comparison of morphology and particle size of asbestos (crocidolite: blue asbestos) (a) and CNT (b) observed by SEM. Fig.10a is crocidolite, one of the asbestos which may cause carcinogenicity most strongly. The diameter of particle is a few nm to a few μm and the length is ranged from submicron to tens of μm. Crocidolite has a distinctly straight needle shape. There are also very fine particles which may easily disperse as dust. The size of CNTs which form bundle is much smaller than asbestos (Fig.10b). The form of CNTs is finer wavy fibers. These indicate the mechanical properties of rigid, non-elastic tendency in crocidolite and easily bending, flexible tendency in CNTs. Asbestos is easily dispersed in air and water, while CNT is difficult to disperse due to the strong tendency to agglomerate.

Asbestos is a kind of clay minerals and silicate in composition. The dissolution level is very low. It is known that asbestos induces mesothelioma after a long-term, large quantity of exposure to respiratory system. This is the result by the different mechanism from that occurred in Ni particles of Fig.5 and related more to the particle size and shape.

Fig.11 is the SEM image of CNTs after immersion in simulated body fluid (SBF) for 2 weeks. Apatite was

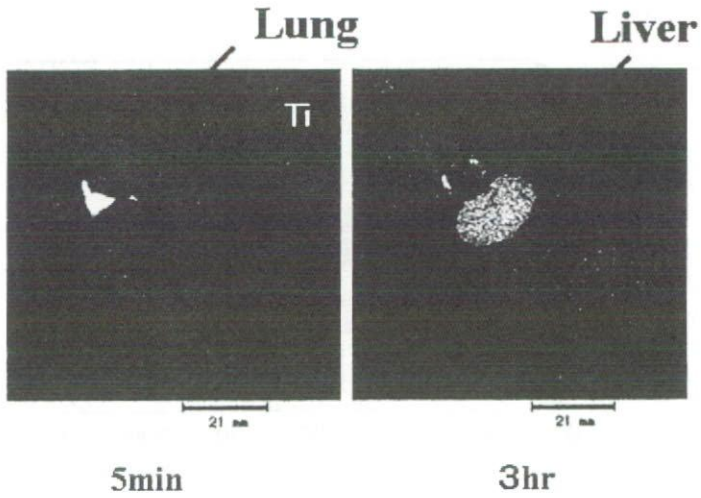

Fig.9 Time course of internal diffusion of 30 nm TiO_2 particles after injection to caudal vein

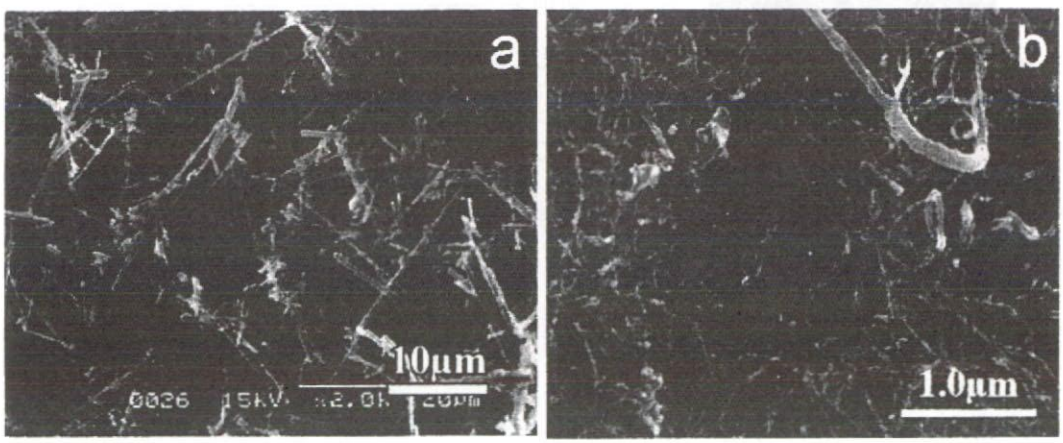

Fig.10 Morphology of asbestos (crocidolite: blue asbestos) (a) and CNT (b) observed by SEM.

precipited on CNT agglomeration. It is known that this kind of so-called biomimetic coating method in SBF gives rise to the formation of calcium phosphate layer on the surface of titanium, which is one of the reasons of excellent biocompatibility of Ti.

When CNTs are immersed in simulated body fluid (SBF), apatite is precipited on CNT. It is known that this kind of so-called biomimetic coating gives rise to the formation of calcium phosphate layer on Ti, which is one of the reasons of excellent biocompatibility of Ti.

Fig.12 is the SEM image of CNTs (long fibers) adsorbed to collagen exposed on dentin surface which was decalcified by etching with acid agent. This shows the nonspecific affinity of CNTs to proteins. CNTs have also affinity to saccharides.

Cell growth cultured on CNTs showed the characteristic behavior. Osteoblast-like cell (SaOS2) is usually grown in a spindle shape. On CNT scaffold, cells are grown fully to the whole direction with numerous fine filopodia at the cell edge.

Fig.13 shows the enlargement of filopodia grown from cell edge on polycarbonate (a) and MWCNT (b) scaffolds observed by SEM. Filopodia are extended far long from cell and combined with CNT meshwork, which shows the high cell adhesivity of CNTs.

Fig.14 is the dental implant composed of hydroxyapatite-coated titanium. Apatite has excellent biocompatibility and induces new bone formation to its surface after implanted in the bone circumstances.

Synthetic hydroxyapatite in the usual case, that is, in a macroscopic size, exhibits excellent osteoconductivity. However it is not substituted to natural bone and remains permanently in the body, therefore it is suitable for the use as implant.

On the other hand it is well-known that natural bone is composed of collagen and nanocrystallites of apatite with the size of approximately 50nm. Fig.15 is the SEM photographs, comparing the difference of morphology of hydroxyapatite for sintered synthetic apatite (a) and natural hard tissue, in this case, enamel of molar of rat (b). In synthetic apatite the size of particles is a few microns and they agglomerate at random, while in enamel enamel prizm of about 5 μm is composed of a bunch of apatite crystallites of about 50nm. It is known that apatite crystallites are grown in their c-axis along collagen fibrils. Thus natural hard tissue is regarded as a kind of composite with the preferably oriented structure of nanocrystallites.

Fig.16 shows the comparison of morphology of hydroxyapatite synthesized without (a) and with (b) collagen by SEM observation. The particle size of apatite is mostly a few microns for without-collagen, while under the coexistence of collagen the product becomes the agglomerate of apatite crystallites of less than 100nm with the lower crystallinity, as revealed from X-ray diffraction analysis.

When the biomimetic nanocomposites of apatite and collagen fibrils were implanted in the subcutaneous tissue, they were covered with fibrous connective tissue and then resorbed mostly at 8 weeks by phagocytosis.

Fig.17 shows the histopathological image when nanocomposites were implanted in the bone marrow of rat for 8 weeks. The area of nanocomposites (asterisks) was decreased and covered with new bone (white asterisks) of lamellar structures. Resorption of the nanocomposites and replacement by new bone proceeded. This tendency was progressed with time by 12 weeks. Phagocytosis of nanoapatite by osteoclasts and osteogenesis by osteoblasts occurred adjacently each other. Resorption and remodeling were similar to the case of autologous bone graft. As a result nanoapatite composites work as bone substitute materials for hard-tissue reconstruction.

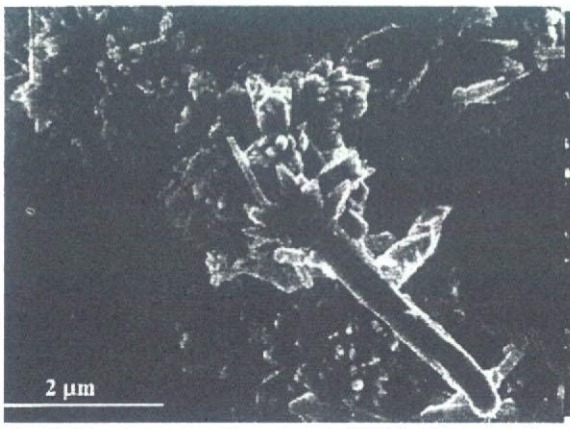

Fig.11 Precipitation of apatite on CNT by biomimetic coating method in SBF.

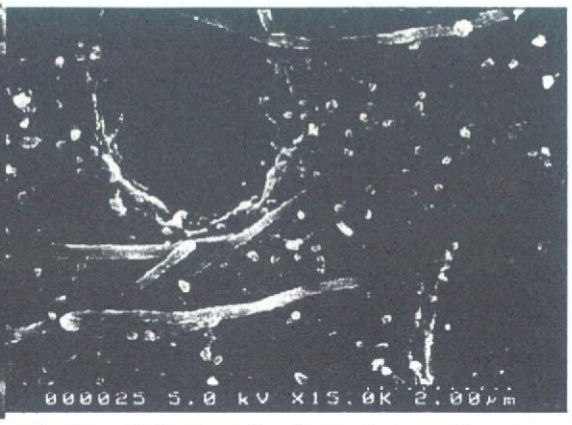

Fig.12 CNTs (long fibers) adsorbed to collagen exposed on dentin surface after etched with acid agent

Discussion

1. Two different effects of nanosizing

Nanosizing effect is usually interpreted in the aspects of the increase of specific surface area. Since chemical reactivity is pronounced with the decrease of particle size, effects related to the ionic dissolution, dominant on biocompatibility of macroscopic materials, accelerate toxicity such as in Ni which generated tumor in the long term implantation for 500nm particles as shown in Fig.5. This effect has the most serious influence, toxicity in many cases, and most commonly taken into account for nanosizing effect. There are, however, other kind of effects. Biocompatible Ti causes inflammation in abraded fine particles [1,2,11], and asbestos [3], a kind of clay minerals, induces mesothelioma after a long-term, large quantity of exposure. These phenomena can be understood as the physical particle and shape effect, apart from the material properties of either toxicity or biocompatibility. Particles below 10 μm cause phagocytosis to cells and inflammation to tissue even for biocompatible materials such as Ti and TiO_2.

2. Invasion of nanoparticles into internal body

By compulsory exposure test, the 30nm TiO_2 particles diffuse directly from the respiratory system into the internal body. Nanoparticles injected from caudal vein diffused with time course to lung, liver and spleen. The uptake of the 30nm TiO_2 particles through the digestive system. was also confirmed. Particles below 50nm might be the objects whose existence has not been assumed by the living body defense system and can invade into the internal body through the respiratory or digestive system.

3. Change from non-resorbable to resorbable apatite by nanosizing

Synthetic hydroxyapatite exhibits excellent osteoconductivity in a macroscopic size, but it is not substituted to bone and remains permanently in the body, therefore it is suitable for the use as implant [12]. It is well-known that natural bone is composed of collagen and nanoapatite crystallites of approximately 50nm [13]. When the biomimetically synthesized nanoapatite composite with collagen [9,14,15] is implanted, phagocytosis and inflammation is induced. Osteoclasts and osteoblasts are then differentiated. Phagocytosis by osteoclasts and new bone formation by osteoblasts is simultaneously activated and proceeded as shown in Fig.17. As a result, nanoapatite composite leads to the bone substitutional properties.

4. Conversion of functions by nanosizing

The conversion of functions is attained for apatite by nanosizing - from osteoconductivity in macroscopic size to bone substitutional properties in nano/micro scale. Nanoparticles cause the reaction of cells/tissue and stimulate to the occurrence of inflammation, which works as toxicity in most cases and, for some cases depending on the situation, pronounces the conversion of functions leading to the bioactive properties. Nano structure is essential for these stages to be processed.

5. Particle behavior of CNT compared with asbestos

There is a possibility to pass through bronchial in the respiratory system for the particles with the size below 10μm. Smaller particles of asbestos can attain pulmonary alveolus through the respiratory system where acute needle shape of asbestos particles makes difficult to be auto-removed. The phagocytosis of acicular

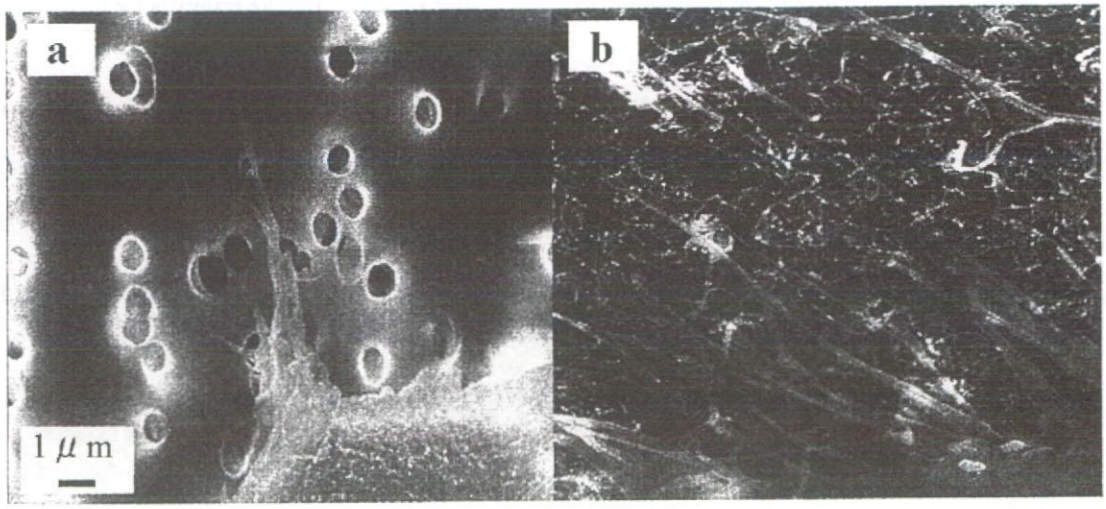

Fig.13 Enlargement of filopodia grown from cell edge on polycarbonate (a) and MWCNT (b) scaffolds

Fig.14 Dental implant composed of apatite-coated titanium

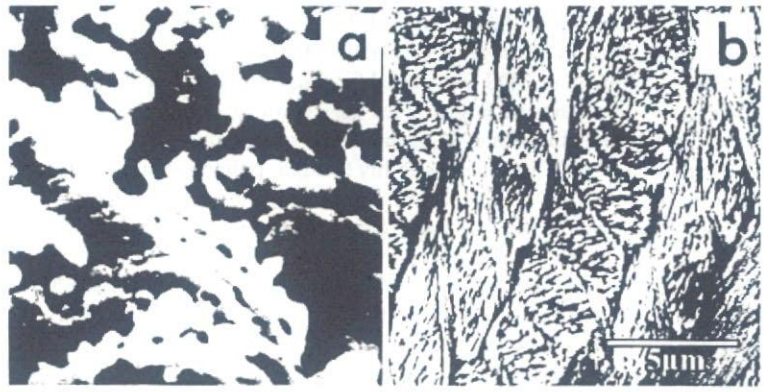

Fig.15 Difference of morphology of hydroxyapatite. a) sintered synthetic apatite, b) enamel of molar of rat.

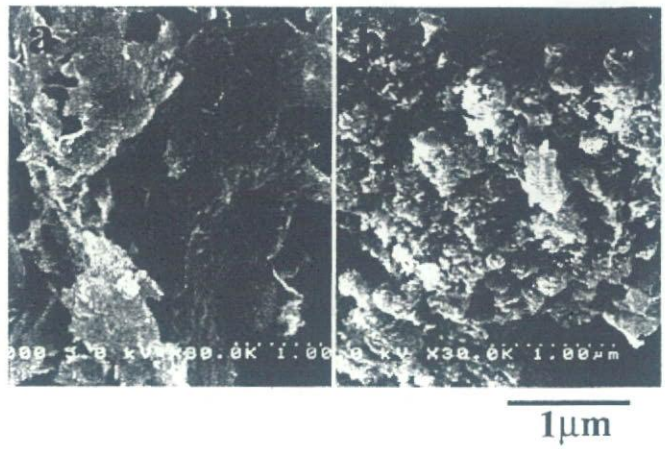

Fig.16 Hydroxyapatite synthesized without (a) and with (b) collagen.

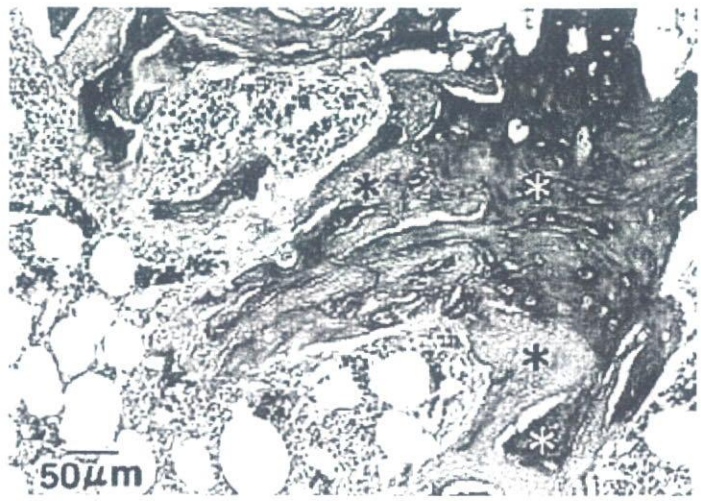

Fig.17 Histological image at 8 weeks after implantation in the bone marrow of rat. Nanocomposites (asterisks) were diminishing and covered with new bone (white asterisks) with lamellar structures [9].

particles is done by macrophages incompletely due to the large longitudinal length. The long term repetition of phagocytosis of accumulated particles leads to the chronic inflammation with superoxide production to attack foreign objects, which in turn causes also defect formation in DNA and results in carcinogenesis.

The development of DDS is expected for the administration of anticancer agent and gene transfection. On the other hand, nanoparticles might be the objects whose existence has not been assumed by living body defense system. They have both sides of high functional nature and stimulus, and their control is important. The size of single particle of CNT has the possibility to attain pulmonary alveolus through the respiratory system.

Particle behavior of CNT compared with asbestos: The present microscopic observation showed that CNT is especially flexible and easily winding around small objects of even μm or less such as bacteria or fine asbestos fibers. CNT is hydrophobic and easily agglomerated, which often causes difficulty to scatter for various applications, while asbestos is hydrophilic and small crystallites are easily dispersible. In a macroscopic view CNT looks as soot which is agglomeration of CNTs. Asbestos is easily dispersed as dust and small single crystallites can be floating in air.

We have found that CNTs have non-specific affinity for saccharides and proteins and also apatite precipitation on the surface when immersed in SBF (Fig.11) [16]. These properties would be the basis for rather favorite properties as biomaterials such as cell adhesion, proliferation and growth (Fig.13) [17-19].

Although the particle size allows the possibility to attain pulmonary alveolus through the respiratory system for both CNT and asbestos, the chemical, physical properties [20-23] and bio-environmental behavior [24-27] of CNT seem different from asbestos.

Conclusion

Particles cause nonspecifically phagocytosis to cells and inflammation to tissue for the size below 3 μm. For the size below 50 nm particles may invade directly into the internal body through the respiratory or digestive system and diffuse inside body. Nanoparticles might be the objects whose existence has not been assumed by living body defense system. Thus the visualization of the internal dynamics of nanoparticles is essential for the proper treatments based on risk assessment and biomedical applications such as DDS. The present study could successfully visualize the internal diffusion of nanoparticles inside the whole body using XSAM.

Nanosizing of materials induces the reaction of cells and tissue and the intrinsic functions of biological organism, which leads to the conversion of functions such as from biocompatibility to stimulus and from osteoconductivity but non-bone substitutional to bone substitutional properties through biological process. This is different from specific surface area effect originated solely from material properties. There are controversial arguments as to whether carbon nanotubes may have the serious toxicity due to their acicular or fibrous particle shape, associated with lung carcinogenicity of asbestos, whilst we have rather found the favorite properties as biomaterials. The physical particle size and shape effect in micro/nanosizing is the essential basis for the proper understanding of such phenomena and for the development of biomedical applications of nanotechnology.

Acknowledgements

Present research was supported by Health and Labour Sciences Research Grants in Research on Chemical Substance Assessment of Ministry of Health, Labour and Welfare of Japan (H18-Chem-General-006).

References

[1] Tamura Y, Yokoyama A, Watari F, Kawasaki T, *Dental Materials J.*, 21 (2002) 355-372
[2] Tamura Y, Yokoyama A, Watari F, Uo M, Kawasaki T, *Mat.Trans.*, 43 (2002) 3043-3051
[3] Watari F, Inoue M, Akasaka T, Sakaguchi N, Ichinose H, Uo M, *Proc.6th Asian BioCeramics Symp.2006* (2006) 142-145
[4] Watari F, Tamura K, Yokoyama A, Shibata K, Akasaka T, Fugetsu B, Asakura K, Uo M, Totsuka Y, Sato Y, Tohji K, "*Handbook of Biomineralization, Vol.3*", Ed. by E.Bauerlein, Wiley-VCH, Weinheim (2007) pp127-144
[5] Kumazawa R, Watari F, Takashi N, Tanimura Y, Uo M, Totsuka Y, *Biomaterials*, 23 (2002) 3757-3764
[6] Tamura K, Takashi N, Kumazawa R, Watari F, Totsuka Y, *Mat.Trans.*, 43 (2002) 3052-3057
[7] Uo M, Watari F, Yokoyama A, Matsuno H, Kawasaki T, *Biomaterials*, 20 (1999) 747-755
[8] Uo M, Tanaka M, Watari F, *J.Biomed.Mater.Res., Part B:Appl.Biomater.*, 70B (2004) 146-151
[9] Yokoyama A, Gelinsky M, Kawasaki T, Kohgo T, König U, Pompe W, Watari F, *J. Biomed Mater Res Part B:Appl Biomater*, 75B (2005) 464-472
[10] Matsuno H, Yokoyama A, Watari F, Uo M, Kawasaki T, *Biomaterials*, 22 (2001) 1253-1262
[11] Zhu Y, Watari F, Dent Mat J., 26 (2007) 245-253

[12] Watari F, Yokoyama A, Omori M, Hirai T, Kondo H, Uo M, Kawasaki T, *Composites Science and Technology*, 64 (2004) 893-908
[13] Watari F, *J.Electron Microscopy*, 54 (2005) 299-308
[14] Liao S, Wang W, Uo M, Ohkawa S, Akasaka T, Tamura K, Cui F, Watari F, *Biomaterials*, 26 (2005) 7564-7571
[15] Liao S, Xu G, Wang W, Watari F, Cui F, Ramakrishna S, C.K.Chan, *Acta Biomaterialia*, 3 (2007) 669–675
[16] Akasaka T, Watari F, Sato Y, Tohji K, *Mat.Sci.Eng.C*, 26 (2005) pp. 675-678
[17] Aoki N, Akasaka T, Watari F, Yokoyama A, *Dent.Mat.J.*, 26 (2007) 178-185
[18] Aoki N, Yokoyama A, Nodasaka Y, Akasaka T, Uo M, Sato Y, Tohji K, Watari F, *J.Biomed. Nanotechnology*, 1 (2005) 402-405
[19] Aoki N, Yokoyama A, Nodasaka Y, Akasaka T, Uo M, Sato Y, Tohji K, Watari F, *Chem. Let.*, 35, 5 (2006) 508-509
[20] Fugetsu B, Satoh S, Iles A, Tanaka K, Nishi N, Watari F: *The Analyst (London)*, 129 (2004) 565-566
[21]I.D.Rosca, Watari F, Uo M, Akasaka T,*Carbon*, 43 (2005) 3124-3131
[22] Ushiro M, Uno K, Fujikawa T, Sato Y, Tohji K, Watari F, Chun W, Koike Y, Asakura K, *Phys. Rev.*, B 73 (2006) 144103/1-11
[23] Wang W, Omori M, Watari F, Yokoyama A, *Dent. Mat. J*, 24(4), (2005) 478-486
[24] Yokoyama A, Sato Y, Nodasaka Y, Yamamoto S, Kawasaki T, Shindoh M, Kohgo T, Akasaka T, Uo M, Watari F, Tohji K, *Nano Letters*, 5 (2005) 157-161
[25] Kiura K, Sato Y, Yasuda M, Fugetsu B, Watari F, Tohji K, Shibata K, *J. Biomed.Nanotech.*, 1 (2005) pp. 359-364
[26] Sato Y, Yokoyama A, Shibata K, Akimoto Y, Ogino S, Nodasaka Y, Kohgo T, Tamura K, Akasaka T, Uo M, Motomiya K, Jeyadevan B, Ishiguro M, Hatakeyama R, Watari F, Tohji K, *Mol.BioSystems*, 1 (2005) pp. 176-182
[27] Sato Y, Shibata K, Kataoka H, Ogino S, Fugetsu B, Yokoyama A, Tamura K, Akasaka T, Uo M, Motomiya K, Jeyadevan B, Hatakeyama R, Watari F, Tohji K, *Molecular BioSystems*, 1 (2005) 142-145

Available online at www.sciencedirect.com
ScienceDirect
Materials Letters 61 (2007) 3624–3628
materials letters
www.elsevier.com/locate/matlet

Morphological effects of variant carbonates in biomimetic hydroxyapatite

Susan Liao [a,b,*], Fumio Watari [c], Guofu Xu [d], Michelle Ngiam [a], Seeram Ramakrishna [a,e], Casey K. Chan [a,b]

[a] Division of Bioengineering, Nanoscience and Nanotechnology Initiative, Faculty of Engineering, National University of Singapore, 117576, Singapore
[b] Department of Orthopaedic Surgery, Yong Loo Lin School of Medicine, National University of Singapore, 119074, Singapore
[c] Graduate School of Dental Medicine, Hokkaido University, Sapporo 060-8586, Japan
[d] School of Materials Science and Engineering, Central South University, Changsha 410083, PR China
[e] Department of Mechanical Engineering, Faculty of Engineering, National University of Singapore, 117576, Singapore

Received 30 October 2006; accepted 5 December 2006
Available online 22 December 2006

Abstract

We prepared nano-carbonated hydroxyapatite (CHA) with different additions of carbonated contents at room temperature. The resulting materials were tested by X-ray diffraction (XRD), Fourier transform Infrared spectroscopy (FTIR), scanning electron microscopy (SEM) and transmission electron microscopy (TEM) respectively. Results were shown that the materials were platelet-like CHA polycrystals that were similar to natural bone minerals, except for the material sample with the highest carbonated content. The presence of carbonated content in hydroxyapatite (HA) significantly decreased the crystallinity of synthesized CHA. Moreover, the morphological change of CHA was observed with the increase of carbonated content. The sequence of morphological change was from flat-like platelet, needle-arrayed platelet, particle-consisted platelet, smaller platelet, and finally spherical particle. This tendency is accordant to controllable solubility of biological HA with certain carbonated content.

Keywords: Carbonated hydroxyapatite; Morphology; Biomimetic; Bone minerals; Nanomaterials

1. Introduction

From a structural point of view, biological apatites are nanosized, with low crystallinity. Isolated mature apatite crystals studied using transmission electron microscopy have clearly shown their platelet-like structures, with average dimensions ranging from 50–100 nm or more in length and 25–50 nm in width [1–5]. Newly deposited crystals are 4–6 nm in thickness. From a compositional point of view, the biological apatites are always carbonated. The HA phase that is presented in natural bone, dentin, and enamel contains approximately 7.4, 5.6, and 3.5 wt.% of carbonate respectively [6]. In the early 1960s, LeGeros [7,8] started to investigate the effect of carbonate on the lattice parameters and morphology of apatite. This is a crucial factor to understand the solubility of biological apatites and the continuous regeneration of bone tissue due to constant dissolution-crystallization cycles.

Recently, scientists tried to prepare nanosized CHA materials via various methods [9–14], in order to control the morphology and chemical composition of HA, which is suitable for the processing of bone-resembling materials with low crystallinity and nanometer sizes. These methods mainly include hydrothermal synthesis, hydrolysis of other calcium phosphates, microwave irradiation, mechano-chemical synthesis etc. All of them yielded stoichiometric, well-crystallized needle-like or rod-like HA powders (size range 20–300 nm) with high crystallinity. However, their morphology and other crystal characteristic are different of that of biological apatites, whereby biological apatites are poorly crystallized and platelet-like.

In this paper, we prepared biomimetic nano-CHA material with variant carbonated content at room temperature. The resulting materials were poorly crystallized and platelet-like as that of biological apatites. The morphological change of CHA with different carbonate contents was investigated using SEM and TEM as well.

* Corresponding author. NanoBioengineering Lab, Nanoscience and Nanotechnology Initiative (NUSNNI), Division of Bioengineering, Faculty of Engineering, Block E3, #05-12, 2 Engineering Drive 3, National University of Singapore, 117576, Singapore. Tel.: +65 65164272; fax: +65 67730339.
E-mail address: bieliaos@nus.edu.sg (S. Liao).

0167-577X/$ - see front matter © 2006 Elsevier B.V. All rights reserved.
doi:10.1016/j.matlet.2006.12.007

2. Materials and methods

Solutions of $CaCl_2$ and H_3PO_4 (mol ratio of Ca/P=1.66) were gradually added into 0.5 M acetic acid separately through respective tube pumps. After 30 min of stirring, a solution of Na_2CO_3 (mol ratio of CO_3^{2-}/PO_4^{3+}=0, 1, 3, 5, 6.7, 8.3, 10) was gradually added. The mixture was further stirred for another 30 min and titrated with sodium hydroxide to pH 9 at room temperature. After the solution was aged for 2 h, the nCHA material was harvested by centrifugation and freeze-dried.

X-ray diffraction (XRD) analysis was performed in a Rigaku/Multiflex diffractometer with the use of Ni-filtered Cu Kα radiation, in the 2θ range of 20°–60° at a scan rate of 2° min^{-1} and with a sampling interval of 0.02°. Full-width at half maximum (FWHM) at (002) and crystallinity were obtained from analysis of XRD data by the MDI JADE6 software [15]. In preparing samples for FTIR analyses, the sample was mixed with KBr in the mass ratio of 1 to 20. Infrared spectra were taken using a Perkin-Elmer system 2000 Fourier transform Infrared spectrometer in the range of 4000–400 cm^{-1}.

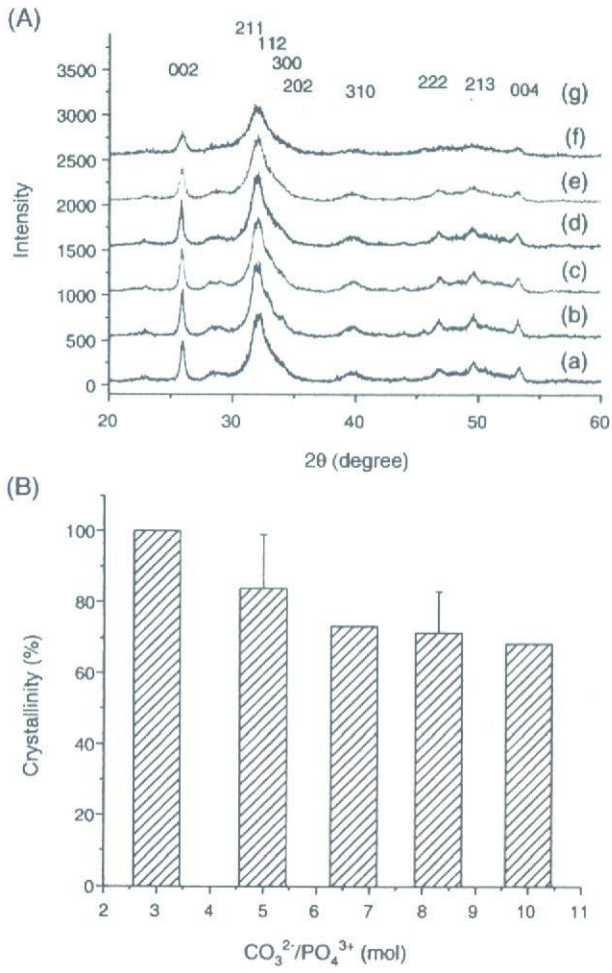

Fig. 1. (A) XRD results of synthesized CHA with variant carbonated contents: (a) CO_3^{2-}/PO_4^{3+}=0; (b) CO_3^{2-}/PO_4^{3+}=1; (c) CO_3^{2-}/PO_4^{3+}=3; (d) CO_3^{2-}/PO_4^{3+}=5; (e) CO_3^{2-}/PO_4^{3+}=6.7; (f) CO_3^{2-}/PO_4^{3+}=8.3; (g) CO_3^{2-}/PO_4^{3+}=10. (B) The crystallinity of synthesized CHA with variant carbonated content.

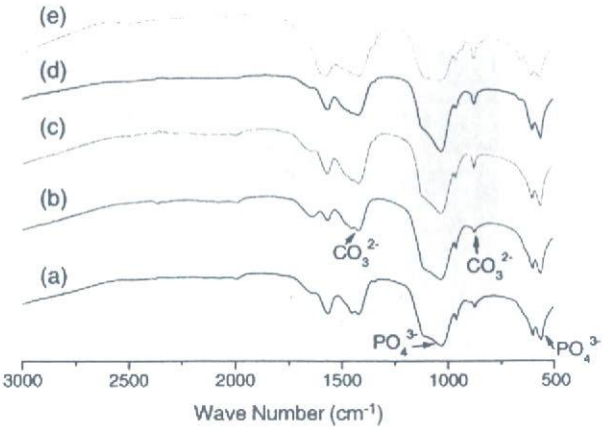

Fig. 2. FTIR spectrum of synthesized CHA with variant carbonated contents. (a) CO_3^{2-}/PO_4^{3+}=0; (b) CO_3^{2-}/PO_4^{3+}=1; (c) CO_3^{2-}/PO_4^{3+}=3; (d) CO_3^{2-}/PO_4^{3+}=5; (e) CO_3^{2-}/PO_4^{3+}=10.

Scanning electron microscopic (SEM) examinations (Sirion 200, FEI Company, USA) were performed after coating the samples with gold. In preparing samples for TEM analyses, the samples were re-suspended in distilled water and then a drop of the suspension was placed on the copper electron microscope grid. After air-drying, each sample was observed on a Hitachi-800 TEM at 150 kV.

3. Results and discussion

The XRD results of all prepared CHA samples with variant carbonated contents were shown in Fig. 1A. Compared to biological apatites which were tested by ourselves (natural bone or teeth [16,17]), the same bone-like characteristics of our materials could be seen: six main peaks with low intensity, one at about 26° indexed to (002), one at 32° referred to broaden and overlapped peaks of (211), (112), (300), (202), one at 40° indexed (310), one at 47° indexed to (222), one at 50° indexed to (213), another at 54° indexed to (004). The extremely broader peak at 32° is quite different with those apatites which are synthesized using other methods, which has separated peaks of (211), (112), (300), and (202). On the other hand, there were no any impurity phases in our samples. If we compare the samples with different carbonated contents in Fig. 1A (a) to (g), the significant broader effect of (002) appeared in (e), (f) and (g). Usually, we calculate the FWHM of this peak to evaluate the crystal size. The more broaden peaks present, the higher the value of FWHM, indicating the lower crystal size of the CHA. In other words, the carbonated substitution in the HA crystal hindered crystal growth, which was concordant to previous reports [7,8,18]. As Fig. 1B illustrated, the calculated crystallinity of CHA was decreased with the augmentation of carbonated content. The FTIR analyses (Fig. 2) detected peaks at the wave numbers representative of the B-type CHA (870, 1430 and 1450 cm^{-1}). Moreover, it also indicated the more significant band at 870 cm^{-1} with increased carbonated content. This intensity of the CO_3-derived bands in the FTIR spectra increased proportionally with the carbonate concentration serving as evidence that the carbonate concentration in the HA lattice could be controlled by varying the carbonate concentration in initial reacted solution.

From XRD and FTIR results, it could be observed that synthesized crystals were all CHA, but the morphologies were rather different from the SEM (Fig. 3) and TEM observations (Fig. 4). Some of these results were also different from the other commonly reported results whereby samples were prepared by the hydrothermal methods and their

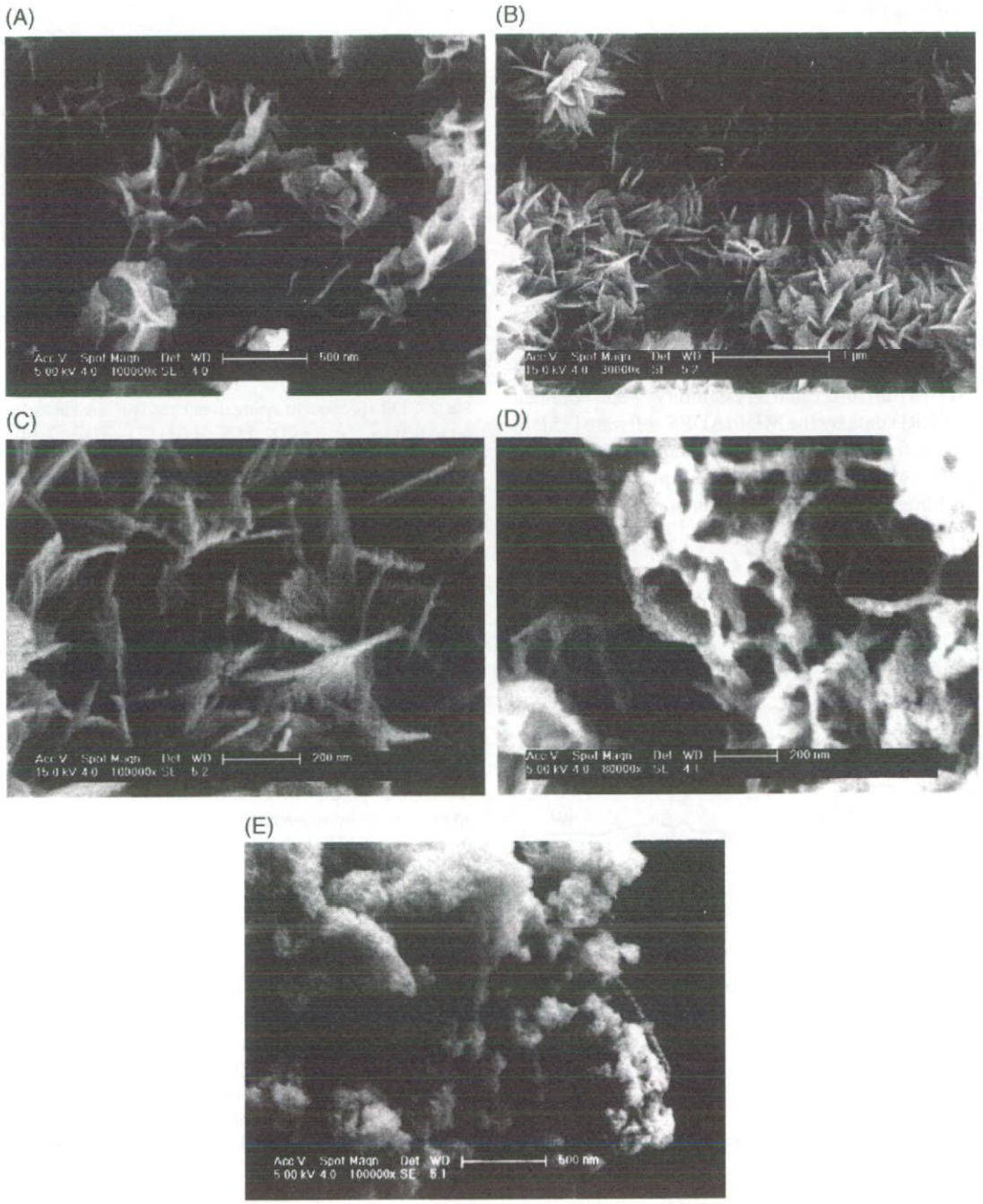

Fig. 3. SEM micrographs of CHA: (A) without carbonated addition; (B) with $CO_3^{2-}/PO_4^{3+} = 1$; (C) is enlarge of (B); (D) with $CO_3^{2-}/PO_4^{3+} = 5$; (E) with $CO_3^{2-}/PO_4^{3+} = 10$.

crystalline morphologies were usually rod- or needle-like. This implies that the different experimental conditions, such as temperature and extent of carbonated additions, might exert important effects on the synthesis of HA. Synthesis at room temperature is an important factor to ensure the low crystal size and low crystallinity. Illustrated in Fig. 3A, the platelet of HA was the initial morphology. With low carbonated content ($CO_3^{2-}/PO_4^{3+} = 1$), the flat platelet changed into needle-arrayed platelet as seen in Fig. 3B and C. The parallel array of needles was also clearly seen in TEM micrograph (Fig. 4A). With the increase of carbonated content ($CO_3^{2-}/PO_4^{3+} = 3$ to 5), the smaller crystals consisting CHA could be expected as depicted in Fig. 4B to C shown. The cracked platelet was also directly observed by SEM (Fig. 3D). Finally, the highest carbonated HA ($CO_3^{2-}/PO_4^{3+} = 10$) became spherical particles, which was demonstrated in Figs. 3E and 4D. To visualize the continuous and dynamic process of morphological change influenced by carbonated content, Fig. 5 schematically illustrates a flow chart on this aspect.

4. Conclusion

We have prepared nano-carbonated hydroxyapatite (CHA) with different carbonated additions to mimic biological apatite.

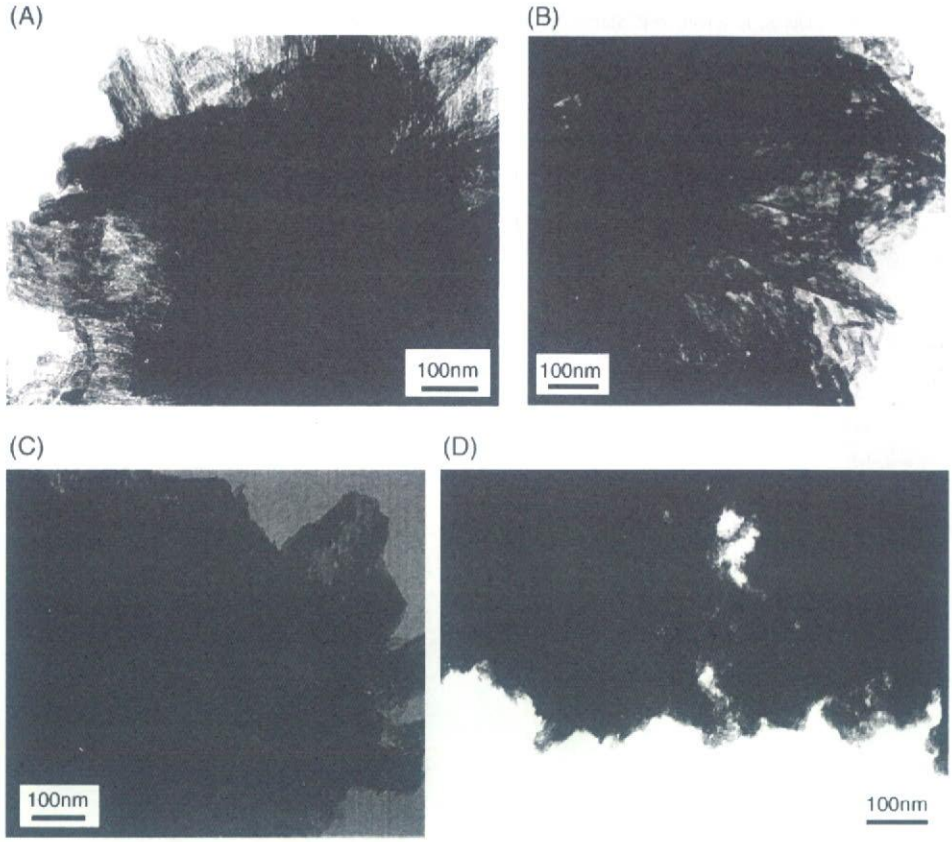

Fig. 4. TEM micrographs of CHA: (A) with $CO_3^{2-}/PO_4^{3+}=1$; (B) with $CO_3^{2-}/PO_4^{3+}=3$; (C) with $CO_3^{2-}/PO_4^{3+}=5$; (D) with $CO_3^{2-}/PO_4^{3+}=10$.

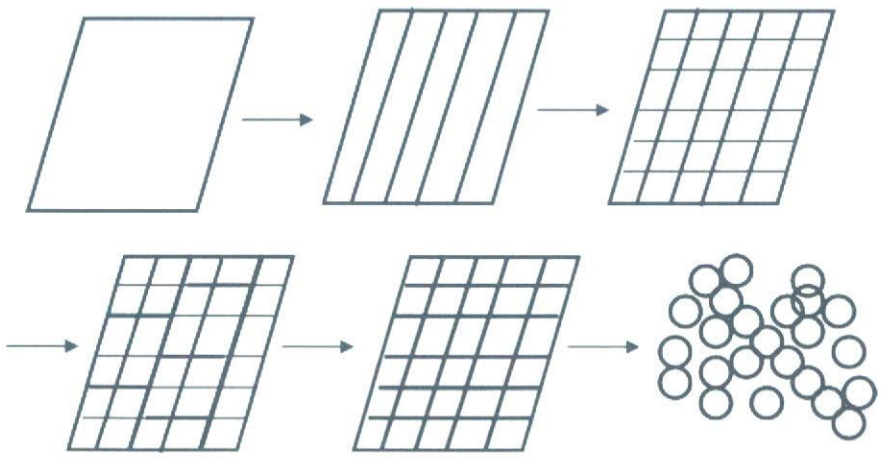

Fig. 5. Schematic diagram of the changing process of CHA morphology with increase of carbonated contents.

They are platelet-like CHA polycrystals with low crystallinity. Moreover, the detailed morphology changed in accordance to the carbonated content. The chronological sequence of morphological change was from flat platelet, needle-arrayed platelet, particle-consisted platelet, smaller platelet, and finally spherical particle.

Acknowledgment

This work was supported in part by the JSPS Post-doctor Program in Japan and NUS LKY PDF fellowship in Singapore.

References

[1] F. Peters, K. Schwarz, M. Epple, Thermochim. Acta 361 (2000) 131.
[2] A. Bigi, G. Cojazzi, S. Panzavolta, A. Ripamonti, N. Roveri, M. Romanello, K. Noris Suarez, L. Moro, Inorg. Biochem. 68 (1997) 45.
[3] W.J. Landis, M.J. Song, A. Leith, J. Struct. Biol. 110 (1993) 39.
[4] H.A. Lowenstam, S. Weiner, On biomineralization, Oxford University Press, New York, 1989, pp. 35–40.
[5] X. Su, K. Sun, F.Z. Cui, W.J. Landis, Bone 32 (2003) 150.
[6] R.Z. LeGeros, Calcium Phosphates in Oral Biology and Medicine, Karger AG, Basel, 1991.
[7] R.Z. LeGeros, Nature 206 (1965) 403.

[8] R.Z. LeGeros, O.R. Trautz, J.P. LeGeros, E. Klein, W.P. Shirra, Science 155 (1967) 1409.
[9] D.G.A. Nelson, J.D.B. Featherstone, Calcif. Tissue Int. 34 (1982) S69.
[10] R.E. Riman, W.L. Suchanek, K. Byrappa, C.W. Chen, P. Shuk, C.S. Oakes, Solid State Ionics 151 (2002) 393.
[11] D. Tadic, F. Peters, M. Epple, Biomaterials 23 (2002) 2553.
[12] W.L. Suchanek, P. Shuk, K. Byrappa, R.E. Riman, K.S. TenHuisenb, V.F. Janas, Biomaterials 23 (2002) 699.
[13] T.S. Sampath Kumar, I. Manjubala, J. Gunasekaran, Biomaterials 21 (2000) 1623.
[14] E. Landi, G. Celotti, G. Logroscino, A. Tampieri, J. Eur. Ceram. Soc. 23 (2003) 2931.
[15] MDI JADE6 software, XRD pattern processing. Materials Data, Inc, 2003.
[16] S.S. Liao, F.Z. Cui, W. Zhang, Q.L. Feng, J. Biomed. Mater. Res. 69B (2004) 158.
[17] S. Liao, F. Watari, M. Uo, S. Ohkawa, K. Tamura, W. Wang, F.Z. Cui, J. Biomed. Mater. Res. 74B (2005) 817.
[18] D.G.A. Nelson, J.C. Barry, C.P. Shields, R. Glena, J.D.B. Featherstone, J. Colloid Interface Sci. 130 (1989) 467.

IOP Publishing Bioinspiration & Biomimetics
Bioinsp. Biomim. 2 (2007) 37–41 doi:10.1088/1748-3182/2/3/001

Systematic fabrication of nano-carbonated hydroxyapatite/collagen composites for biomimetic bone grafts

Susan Liao[1,2], Michelle Ngiam[1], Fumio Watari[3], Seeram Ramakrishna[1,4] and Casey K Chan[1,2]

[1] Nanoscience and Nanotechnology Initiative, Division of Bioengineering, Faculty of Engineering, National University of Singapore, 117576, Singapore
[2] Department of Orthopaedic Surgery, Yong Loo Lin School of Medicine, National University of Singapore, 119074, Singapore
[3] Graduate School of Dental Medicine, Hokkaido University, Sapporo 060-8586, Japan
[4] Department of Mechanical Engineering, Faculty of Engineering, National University of Singapore, 117576, Singapore

E-mail: bieliaos@nus.edu.sg

Received 3 January 2007
Accepted for publication 19 March 2007
Published 22 June 2007
Online at stacks.iop.org/BB/2/37

Abstract

A novel biomimetic self-assembly method was designed to create nano-carbonated hydroxyapatite/collagen (nCHAC) composites by means of incorporating various collagen and carbonate concentrations using solutions such as $CaCl_2$, H_3PO_4, and Na_2CO_3. At a given range of collagen and carbonate content, the nanosized inorganic phase of the newly synthesized material has a low degree of crystallinity which resembles that of natural bone. By manipulating the concentrations of collagen and carbonates, various morphologies of the nCHAC can be obtained. The crystal size of nCHAC is dependent on the concentration of carbonate and collagen present in the composites. For instance, higher collagen concentration results in smaller crystal nCHAC crystal size. Conversely, the higher the carbonate content, the smaller are the crystal size and the collagen fibril assembly. As the carbonate content increased, the plate-like crystals first became needle-like structures, subsequently short needle-like crystals and eventually became spherical particles. From this study, our method showcased the flexibility of fabricating various types of nCHAC composites which can be designed for different bone applications.

Introduction

It is known that human bone is an extracellular matrix mainly composed of 65% hydroxyapatite (HA) nanocrystal and 25% collagen (COL) fibers. In dentine, the composition is about 70% HA and 20% COL. HA nanocrystals aligned their C-axes along COL fibers. In an earlier study, nano-HA/COL (nHAC)-based composites were prepared using the self-assembled co-precipitation method whereby the HA was similar to that of natural bone [1–3]. It is known that the collagen assembly process greatly affects mineral formation, including the HA crystal size and controlled carbonated content, but the exact mechanism is still unclear. In other words, it is not known whether the highly carbonated mineral is similar to the pure HA mineral when combined with molecular collagen.

Scientists have attempted to prepare nanosized CHA materials by various methods, in order to control the morphology and chemical composition of HA, aiming to achieve low crystallinity and nanometer crystal sizes that would be suitable for the processing of bone-resembling materials [4–7]. In addition, controlling the level of carbonate substitution in HA is a convenient way to change the solubility and morphology of the synthesized CHA crystals, which subsequently affect the properties of the HA-based biomaterials [8]. However, the co-effect of the carbonated

components and collagen in nano-CHA/COL (nCHAC) composites is currently debatable.

In recent years, the biomimetic mineralized collagen material, widely known as the nanoapatite/collagen composite which is prepared by different methods, has drawn the attraction of many researchers [1, 2, 9]. Because of its excellent biodegradation properties and superb biocompatibility as a biomimetic component and exhibiting nanostructure of natural bone, it is desirable for the stimulation and regeneration of new bone formation [10–12]. We have already reported the possible synthesis method for the nCHAC composite that is the co-precipitation in aqueous solution [13, 14]. Although the nCHAC composite proved to be promising based on favorable preliminary results, much work is needed in order to obtain a controllable mineralization of the nano-HA and extracellular matrix (ECM) that resembles natural hard tissue. This will provide us with fresh insights of nano-HA/collagen characters and relationships with natural hard tissue growth. Moreover, precise fabrication of such materials would be made possible to meet the different implant requirements for clinical applications. In this study, we further investigated the morphological changes with respect to the various carbonate and collagen contents in the nCHAC composite.

Materials and methods

Type I atelocollagen gel (2 wt%, Koken Company, Japan) (2.5 and 5 g) was added to 0.5 M acetic acid. Next, solutions of $CaCl_2$ and H_3PO_4 (Ca/P = 1.66) were gradually added separately through respective tube pumps; after 30 min of stirring, a solution of Na_2CO_3 (mol ratio of $CO_3^{2-}/PO_4^{3+} = 0$, 1, 3, 5, 6.7, 8.3, 10) was gradually added. The mixture was stirred for another 30 min, and titrated with sodium hydroxide to pH 9 at room temperature. After the solution was aged for 2 h, the nCHAC material was harvested by centrifugation and freeze-dried. Henceforth, no 1# refers to the nCHAC consisting of 2.5 g collagen gel and materials with mol ratio of CO_3^{2-}/PO_4^{3+} of 0, 1, 3, 5 and 10 are denoted as 10#, 11#, 12#, 13# and 14#, respectively. nCHAC denoted as no 2# refers to the nCHAC consisting of 5 g collagen gel and those with a mol ratio of CO_3^{2-}/PO_4^{3+} of 0, 1, 3, 5 and 10 are identified as 20#, 21#, 22#, 23# and 24#, respectively.

CHA material without collagen was prepared by the same process, which served as a control (C#). Likewise, in this control group, C0#, C1#, C2#, C3#, C4# refer to materials with a mol ratio of CO_3^{2-}/PO_4^{3+} of 0, 1, 3, 5 and 10, respectively. A summary of the identification of the materials used is shown in table 1.

X-ray diffraction (XRD) analysis was performed in a Rigaku/Multiflex diffractometer with the use of Ni-filtered Cu Kα radiation, in the 2θ range of 10°–80° at a scan rate of 2° min^{-1}, with a sampling interval of 0.02°. The data were analyzed using the MDI JADE6 software [15]. The diffraction peaks broadening by small crystallites can be semiquantitatively estimated by the Scherrer equation: $\beta_{1/2} = K\lambda/(D\cos\theta)$ [16]. Here, $\beta_{1/2}$ is the full-width at half maximum in 2θ that can be automatically calculated by MDI JADE6 software, K is a constant set to 1, λ is the x-ray wavelength in angstroms, D depicts the average crystallite size and θ is the diffraction angle of the corresponding reflex.

Table 1. Numbers of prepared nCHAC composites.

Series	Collagen gel (g)	CO_3^{2-}/PO_4^{3+} (mol) = 0	1	3	5	10
Control	0	C0#	C1#	C2#	C3#	C4#
1#	2.5[a]	10#	11#	12#	13#	14#
2#	5[a]	20#	21#	22#	23#	24#

[a] Final weight percentage of collagen is about 8% in 1# and about 16% in 2#.

The sample was mixed with KBr in the mass ratio of 1 to 20. Infrared spectra were taken using a Perkin–Elmer system 2000 Fourier transform IR (FTIR) spectrometer in the range of 4000–400 cm^{-1}. The carbonated weight percentages were measured through TGA by Rigaku Thermoflex TG8110/TAS100 (weight loss from 600 °C to 1000 °C [7, 19]). Samples were heated from room temperature to a maximum temperature of 1000 °C in increments of 10 °C min^{-1}. In preparing samples for TEM, the sample was re-suspended in distilled water and a drop of the suspension was placed on the copper electron microscope grid. After air-drying, the sample was observed on a Hitachi-800 TEM at 150 kV. Another method is to drop the aged reaction solution before freeze-drying on the copper grid.

Scanning electron microscopy (SEM) examinations (Sirion 200, FEI Company, USA) were performed after coating the samples with gold. A combined energy dispersed spectrometer (EDAX) system (Genesis 60S, EDAX Inc., USA) with this SEM allowed us to calculate the values of Ca/P ratio and N as a percentage in the nCHAC samples ($n = 6$).

Results and discussion

Consider the initial mineralization *in vivo*: the collagen provides superfluous positions for calcium nucleation. In other words, the ratio of collagen and apatite is very high at that time. Consequently, in the following remodeling of calcified tissue, the ratio of collagen and apatite decreased or became stable. Our biomimetic nano-HA/collagen-based composite has exhibited certain similarities to natural bone based on the innumerable positive *in vitro* and *in vivo* results obtained. We postulated the importance of such similarities between synthetic nano-HA/collagen and natural bone ECM in order to enhance these characteristics. The initial crystal development stemmed from nano-HA to nano-CHA in the composite, and different collagen contents simulate the different stages of mineralization as previously mentioned. In this respect, we successfully fabricated a series of nCHAC composites by varying the collagen and carbonated contents in aqueous solutions.

EDAX results confirmed the varied contents of HA in the composite, which showed that the N at% in 1# was in the range of 3.5–4.7% and that in 2# was in range of 5.2–6.9% (table 2). Although the Ca/P ratio from EDAX was not exactly 1.67

Table 2. N at% in 1# and 2# nCHAC composites (EDAX).

	CO_3^{2-}/PO_4^{3+} (mol) =				
	0	1	3	5	10
1#	4.5	3.6	4.7	3.5	4.6
2#	6.2	6.6	5.2	6.9	6.6

Table 3. Ca/P ratio in 1# and 2# nCHAC composites (EDAX).

	CO_3^{2-}/PO_4^{3+} (mol) =				
	0	1	3	5	10
1#	1.42	1.42	1.47	1.44	1.43
2#	1.47	1.42	1.46	1.51	2.35

Table 4. Carbonated component percentage in 1# and 2# nCHAC composites (TGA).

	CO_3^{2-}/PO_4^{3+} (mol) =				
	0	1	3	5	10
1#	2.8	2.9	3.6	6.9	14.7
2#	4.8	5.8	7.1	7.0	11.7

(table 3), the phase of resulting composites was nano-CHA, which was the same phase present in bone and dentine that has been reported [13]. Herein, we did not list each x-ray curve of all samples. In B-type of CHA, some of the phosphate positions would be replaced by the carbonated groups. The slight change of Ca/P ratio in the composites is reasonable. However, the Ca/P ratio from EDAX results demonstrated the stable crystalline phase in the composite except for materials with a higher collagen content and mol ratio of CO_3^{2-}/PO_4^{3+} (24#). As the nano-size crystal induced the extremely broad peak of the x-ray curve as seen in materials with high collagen content and CO_3^{2-}/PO_4^{3+} (24#), it was difficult to identify the exact phases. The Ca/P ratio of 24# (2.35) that was higher than other samples demonstrated that 24# included a Ca-contained phase without P other than HA. From this point, we know that the Ca/P present in 24# might well be above the range of biological apatite.

Therefore, we considered the carbonated percentage of nCHAC composites with the above results. The carbonated percentage in 1# nCHAC composite was continuously increasing in 1# from 2.8% (10#) to 6.9% (13#), then 14.7% (14#) (table 4). The FTIR results (figure 1) also illustrated this increasing trend. The type-B CHA was seen in all nCHAC composites. For the nCHAC composite with a higher collagen concentration (#2), the carbonate content was stabilized at approximately 7% for materials with CO_3^{2-}/PO_4^{3+} mol ratios of 3 and 5 (22# and 23#). Besides CHA, additional phases were possibly formed in materials with a high CO_3^{2-}/PO_4^{3} mol ratio of 10 (14# and 24#) regardless of collagen concentration. It is widely known that the biological apatite in natural bone, dentine and enamel contains approximately 7.4, 5.6 and 3.5 wt% of carbonate, respectively [18]. This is indicative that an *in vivo* environment can control the carbonated content in nano-HA for precise requirements. Conversely, this

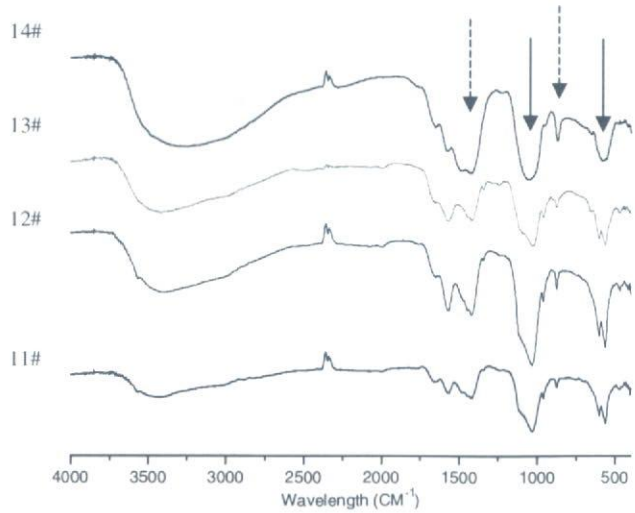

Figure 1. FTIR results of 1# series nCHAC composites (11#, 12#, 13#, 14#). The arrows refer to the phosphate groups, and the dashed arrows refer to the carbonated groups.

(This figure is in colour only in the electronic version)

Table 5. Average crystal size (nm) in 1# and 2# nCHAC composites ((0 0 2) peak of XRD).

	CO_3^{2-}/PO_4^{3+} (mol) =				
	0	1	3	5	10
0#	24.28	26.48	23.53	26.88	22.36
1#	22.87	23.05	23.96	27.78	NA[a]
2#	17.12	14.61	16.09	18.08	NA[a]

[a] The average crystal size of 14# and 24# could not be calculated for the unavailable and separated peak at about 26° (0 0 2). However, another characteristic broad peak at about 32° (2 1 1, 1 1 2, 3 0 0, 2 0 2) of nHA was shown.

control can be achieved by the artificial method used in this study.

Regardless of the carbonate present, the nano-scale synthesized CHA in the composites were maintained. The data on the crystal size for all the materials are shown in table 5. Without collagen, although the size of [0 0 2] of C# were still several nanometers from XRD (table 5), SEM/TEM observations have shown that the crystal sizes of resulting materials reached a micrometer-scale. With collagen, it was shown that the crystal sizes of nCHAC (2#) with high collagen content were lower than that of 1# which had a lower collagen content, as seen from the calculation results from XRD data (table 5). 1# was above 23 nm but 2# was only 16 nm in the *c*-direction (0 0 2). However, there was no significant difference in the crystal size among the samples with different carbonate contents. From these observations, it is possible to prepare samples with different crystal parameters by the variation of the collagen addition rates. From the report of Tadic [5], the bone samples have essentially the same anisotropic crystal size, i.e. about 25 nm in the *c*-direction (0 0 2). The low crystalline size of CHA was mainly controlled

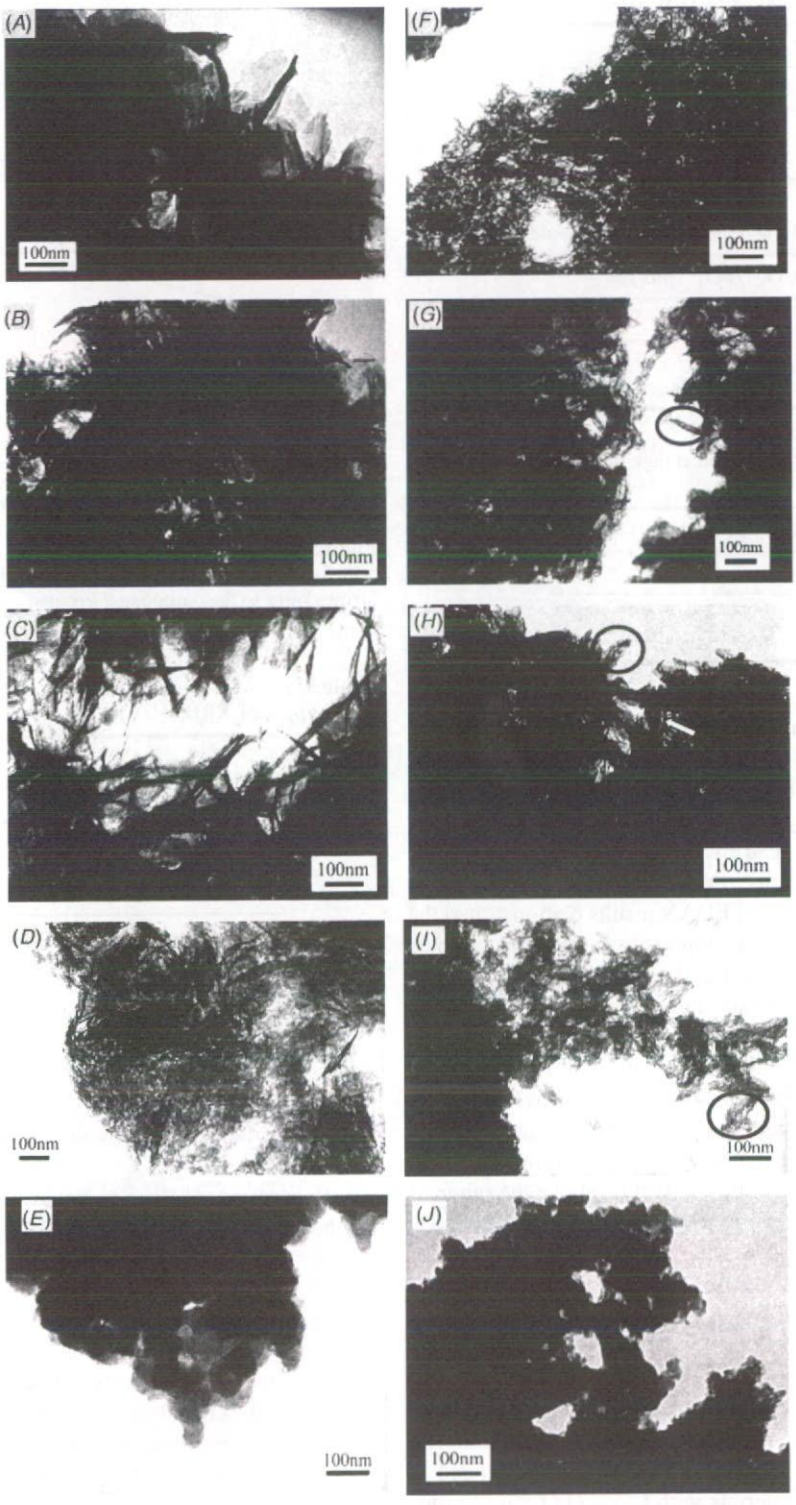

Figure 2. (*A*)–(*E*) are TEM photographs of 10#, 11#, 12#, 13# and 14#, respectively. (*F*)–(*J*) are TEM photographs of 20#, 21#, 22#, 23# and 24#, respectively. The black circles represent the assembled unit of the nCHAC composite.

by the collagen content as our studies have demonstrated, which can explain the observation of the small crystal size of nCHA in immature bone tissue. This organic component-collagen not only directed the CHA synthesis *in vivo*, but also the self-assembly of ordered nanofibers with unique patterns [19, 20].

The morphologies of biomimetic nCHAC composites affected by the collagen and carbonate components and